The influence of the enhancement of the convective activities of tropical Pacific on the trend of stratospheric sudden warmings in the period of 1948-2003

Yuanpu Li
Fudan University

Zhiping Wen (zpwen@Fudan.edu.cn)
Fudan University https://orcid.org/0000-0003-1259-0362

Research Article

Keywords: SSW, tropical convective activities, planetary wave

Posted Date: April 13th, 2021

DOI: https://doi.org/10.21203/rs.3.rs-390163/v1

The influence of the enhancement of the convective activities of tropical Pacific on the trend of stratospheric sudden warmings in the period of 1948-2003

Yuanpu Li[1], and Zhiping Wen[1*]

1 Institute of Atmospheric Sciences, Fudan University, Shanghai, China

*Corresponding author:

Zhiping Wen

Institute of Atmospheric Sciences, Fudan University, Shanghai, China

Email: zpwen@fudan.edu.cn

Abstract

The exploration of the trend of stratospheric sudden warming (SSW) in the Northern Hemisphere is conducive to predict SSWs in the future. Utilizing the National Centre for Environmental Prediction (NCEP) (1948-2017) and Japanese 55-year reanalysis data (JRA55) (1958-2017), we investigated the duration and strength of SSWs in the Northern Hemisphere winter (December-February). We found the duration of SSWs has an increasing trend and the strength of SSWs tends to strengthen from 1948 to 2003. However, after 2003, these trends did not continue. We also utilize the observed cloudiness from the International Comprehensive Ocean-Atmosphere Data Set (ICOADS) to examine the convective activities in the tropical Pacific and found that the convective activities in the tropical central Pacific are enhanced during the period of 1948-2003, and the trend of the enhancement of the convective activities ceases after 2003. The circulation anomalies caused by the enhanced convective activities propagate to the troposphere at high latitudes through wave trains. The anomalies of circulation and the climatic circulation at high latitudes interfere with each other and superimpose, which has a significant impact on planetary wave 1 (PW1). As a result, the PW1 in the troposphere also showed an increasing trend from 1948 to 2003 and a decreasing trend after 2003. After the stratosphere filters out the planetary wave with a large wavenumber, PW1 accounts for more proportion of planetary waves, which causes the trend of SSW to change synchronously.

Keywords: SSW; tropical convective activities; planetary wave

1. Introduction

Stratospheric sudden warming (SSW) is one of the important weather processes that can affect the troposphere in winter (Baldwin et al. 2021). The stratospheric polar vortex has formed in the Arctic stratosphere after autumn, and the polar vortex is strongest during the polar night (Waugh et al. 2017). However, this highly spinning weather system will be disrupted by SSWs, during which the upward propagating planetary waves cause the stratospheric polar vortex to shift, split, or even collapse (Charlton and Polvani, 2007) and the temperatures in the polar region could rise by more than 30 K in a few days (Butler et al. 2015). WMO/IQSY (1964) has defined two types of SSW, major warming and minor warming. If the temperature gradient between 60° N and the pole reverses and the zonal-mean zonal wind at 60° N, 10 hPa reverses from westerly to easterly, the event is defined as major warming (Andrew, 1987). The major warming requires a reversal of the zonal winds of 60° latitude, while the minor warming doesn't. Studies show that some SSWs have significant influences on the troposphere on the timescale of weeks to decades (e.g., Baldwin and Dunkerton, 2001; Thompson and Wallace, 2001; Reichler et al. 2012). The circulation systems affected by SSWs include the Arctic Oscillation and Northern Annular Mode (NAO) (e.g., Baldwin and Dunkerton, 1999; Domeisen 2019), midlatitude blocking systems (e.g., Mitchell et al. 2013; Davini et al. 2014), and cold-air outbreaks in China (e.g., Kolstad et al. 2010; Lu and Ding, 2015). Although Some minor warmings occurred in the Northern Hemisphere (Wang and Chen; 2010) and Southern Hemisphere (Hendon et al., 2019; Rao et al., 2020) did not meet the standard of major warming, these minor warming were also related to the weather anomalies in the troposphere, such as the

bushfires in Australian (Lim et al., 2019).

Since SSWs have the potential to influence the weather and climate in the northern hemisphere winter, SSWs have received extensive attention from the science community, who want to find out whether there is any long-term trend in SSWs. There is high uncertainty in SSW trends simulated by models, e.g., simulations driven by the same greenhouse gases scenario obtain opposite trends of SSW frequency (e.g., Butchart et al. 2000). Although recent model simulations showed that the increase of greenhouse gases after the industrial revolution would induce more SSWs (e.g., Schimanke et al. 2013), there is no significant increase in SSW frequency detected in the observation data until now. Domeisen (2019) inversely reconstructed the time series of SSW frequency since 1850 by utilizing the observed NAO index, which shows that there is high uncertainty in the SSW frequency and there is no trend of SSW frequency. Wang et al. (2017) analyzed the NCEP/NCAR reanalysis dataset and stated that from 1953 to 2016, the frequency of SSW events did not increase or decrease significantly. The result by Wang et al. (2017) is consistent with the previous research by Charlton and Polvani (2007), which stated that between 1960s and 2000s, the number of SSWs did not show a recognizable trend. Charlton and Polvani (2007) attributed this difficulty of identifying the trend of SSWs partly to the lack of SSWs in certain periods such as the 1990s. Although previous studies analyzed the frequency of SSW, other characteristics of SSW, such as the trends in duration and strength, have not been analyzed. When analyzing interdecadal changes in SSWs, Li et al. (2018) combined the minor warmings and the major warmings together to analyze, in order to overcome the

shortcoming of sample size is too small. The reason why these two types of SSW can be analyzed together is that the dynamics of major warming and minor warming are quite similar (Holton, 1976; Matsuno, 1971; Quiroz, 1986). This article uses the same method in Li et al. (2018) to study the trend of SSWs from the perspectives of duration and strength.

Many studies have found SSWs are influenced by the changes in tropical convective activities caused by sea surface temperature (SST) anomalies (Horel and Wallace, 1981; Brönnimann, 2007; Zhou et al. 2014; Zhang et al. 2015) or the changes caused by the intraseasonal variability such as Madden-Julian Oscillation (MJO) (Garfinkel and Schwartz 2017). The vorticity perturbations triggered by the tropical convective activities propagate poleward and modulate planetary waves in the high latitude (Gill, 1980; Seo and Son, 2012; Lukens et al., 2017). Some other studies show that the SSWs are also impacted by El Niño (Bell et al. 2009; Garfinkel and Hartmann, 2008; Li and Tian, 2017). SST variations in the extratropical Pacific can influence SSWs as well. Pacific Decadal Oscillation (PDO) (Mantua et al. 1997), which is the first mode of North Pacific SST anomalies, and Victoria mode, which is the second mode of North Pacific SST anomalies are reported to be capable to modulate the interannual variations of SSWs (Bond et al. 2003; Woo et al. 2015; Li et al. 2018; Hu et al. 2018). Though it is difficult to relate a single SSW event with solar activity, evidence shows that solar activity would modulate stratospheric winds, which are related to the conditions for the tropospheric planetary waves to be transported to the stratosphere. The planetary waves propagating to the stratosphere from the troposphere are essential for SSWs, which are

altered by the phase change of the Solar cycle (Kodera 1991). The polar night jet, which would change dramatically before and after SSWs, is influenced by solar activity as well (Kuroda et al. 2002). The influences of the factors, including convective activities in tropical Pacific, SST in the tropical and extratropical Pacific, solar activities, on the trend of SSWs are discussed in this paper.

This paper has investigated the trends of SSWs in the Arctic stratosphere from the perspectives of duration and strength. The factors driving the changes in the trends of SSWs are investigated, and the contribution of the factors to the trends of SSWs and planetary waves are also analyzed. Section 2 introduces the datasets and methods. The trends of SSWs and convective activities in the tropical Pacific are described in Section 3. Section 4 analyzes the mechanism of convective activities in the tropical Pacific impacting the stratospheric planetary waves. Discussion and conclusion are given as section 5.

2. Data and method

a. Data

The meteorological fields are the National Centre for Environmental Prediction (NCEP) reanalysis dataset (Kalnay et al. 1996), which has a horizontal resolution of 2.5°×2.5° and covers the period from 1948 to 2018. The Japanese 55-year (JRA55) Reanalysis dataset (Kobayashi et al. 2015; Harada et al. 2016) with a horizontal resolution of 2.5°×2.5° is utilized to verify the trends of SSWs. The change of tropical convective activities for the last 70 yr cannot be directly described from the

precipitation or Outgoing Longwave Radiation (OLR) observations, since the observations are quite rare in the eastern Pacific before the satellites are used. An alternative is to investigate the cloudiness, which is the total cloud amount from the observations of International Comprehensive Ocean-Atmosphere Data Set (ICOADS) (Woodruff et al. 2011) (https://data.nodc.noaa.gov/icoads/). The precipitation data for comparison and verification is derived from GPCP Version 2.3 Combined Precipitation Data Set for 1979-2017 (Adler et al. 2017). The solar irradiance is the radio emission from the Sun at a wavelength of 10.7 centimeters averaged over the month provided by Natural Resources Canada (http://www.spaceweather.ca/solarflux/sx-5-eng.php).

b. Definitions

The duration of SSWs is the number of days when the gradient of temperature between 60°–90°N at 10 hPa becomes positive. The strength of SSWs is defined as the maximum of the gradient of temperature between 60°–90°N at10 hPa. Since in the years of 1948, 1949, 1952, 1954, 1955, 1956, 1957, 1960, 1963, 1966, 1969, 1975, 1985, 1996 and 2010, there are not any SSW, then the duration of SSWs should be 0 day. The maximum of the temperature gradient of these winters are below 0 K/degree, although the maximum of the temperature gradients of these winters don't represent SSW strength, in order to keep the continuity of the time series when calculating the trend of strength, the temperature gradients of these winters are kept and shown as blue bars in Fig. 1b. The definition of SSWs based on temperature gradient would include both major and minor SSWs, which are not distinguished in this study. The winter is referred to December to February.

The first leading mode (PC1) and the second leading mode (PC2) of winter North Pacific SST is calculated by the empirical orthogonal function (EOF) analysis following Li et al. (2018). PC1 and PC2 represent PDO and Victoria mode of winter North Pacific SST respectively.

The atmospheric heat source cannot be directly observed, while it can be measured with the reverse method by regarding the net heat source as remanding term in the thermodynamic conservational equation. According to Ding (1989), the heat source Q1 is

$$Q_1 = c_p \left[\frac{\partial T}{\partial t} + V \cdot \nabla T + \left(\frac{P}{P_0}\right)^{\kappa} \omega \frac{\partial \theta}{\partial p}\right] \quad (1)$$

Where $P_0 = 1000$ hPa, $\kappa = R/C_p$, R, and Cp are the gas constant and the specific heat at constant pressure of dry air, and θ is the potential temperature. Integrating Eq. (1) from 100 hPa to the surface pressure *Ps*, we obtain

$$\langle \mathrm{Q}_1 \rangle = \frac{1}{\mathrm{g}} \int_{100}^{p_s} \mathrm{Q}_1 \mathrm{d}_p \quad (2)$$

The monthly indices of Pacific North America Pattern (PNA) and Western Pacific (WP) are calculated by the Rotated Principal Component Analysis (RPCA) (Barnston and Livezey 1987), downloaded from NOAA Climate Prediction Center.

In order to diagnose the strength of planetary wave, the Eliassen–Palm fluxes (EP fluxes) are calculated in log-pressure coordinates using the method given by Andrews et al. (1987):

$$F^{(\phi)} = \rho a \cos\phi \left(\frac{\overline{v'u'}}{\theta_z}\overline{u}_z - \overline{v'u'}\right) \quad (3)$$

$$F^{(z)} = \rho a \cos\phi \left[\left(\mathrm{f} - \frac{1}{a\cos\phi} (\bar{\mathrm{u}}\cos\phi)_{\phi} \right) \left(\overline{v'\theta'} \right) / \overline{\theta}_z - \overline{w'u'} \right] \quad (4)$$

The divergence of EP fluxes is defined as

$$\nabla \cdot \mathrm{F} = \frac{1}{a\cos\phi} \frac{\partial}{\partial\phi} (\mathrm{F}^{(\phi)}\cos\phi) + \frac{\partial}{\partial z} (\mathrm{F}^{(z)}) \quad (5)$$

Where a is the mean of Earth radius, z is the height in the log-pressure coordinate, ϕ is latitude, H is the mean scale height of the atmosphere, $\rho = \rho_s \exp(-z/H)$ is the standard air density in log-pressure coordinates, ρ_s is the reference air density at sea level.

c. Statistics

Climate variables (e.g., the duration of SSW or PW1) can be represented by statistical random variables, X. X linked over time would form a stochastic process, $X(i)$. A simple equation is

$$X(i) = X_{trend}(i) + X_{noise}(i) \quad (6)$$

In Eq. (6), a climate variable is decomposed into trend and noise components. The expectation value of noise component is zero. The location center of the climate variable is represented by the trend, $X_{trend}(i)$. The linear regression is a simple and convenient method to describe $X_{trend}(i)$ by the slope, $\beta 1$. The equation is

$$X(i) = \beta_0 + \beta_1 \times T(i) + X_{noise}(i) \quad (7)$$

$T(i)$ is the time variable corresponding to $X(i)$. The ordinary least-squares estimation is used to minimize the sum of squares of differences between $X(i)$ and the linear fit. $\beta 1$ is described as the trend rate of $X(i)$. The detail can be found in Mudelsee (2019).

Multiple Linear Regression is utilized to estimate the contribution of the independent variables to the trend of the climate variable. These variables, including the indices of cloudiness, the first leading mode (PC1) and the second leading mode (PC2) and the solar irradiance, are verified to be statistically independent with each other according to the correlation coefficient. The equation is

$$Y(i) = \alpha_0 + \alpha_1 \times X_1(i) + \alpha_2 \times X_2(i) + \alpha_3 \times X_3(i) + \alpha_4 \times X_4(i) + Y_{noise}(i) \quad (8)$$

The ordinary least-squares estimation is utilized to minimize the sum of squares of differences between $Y(i)$ the linear fit. $Y(i)$ is a climate variable, which can represent SSW duration, SSW strength, PW1, or PW2 in the following analysis. X_1, X_2, X_3, X_4 is the time series of cloudiness, the first leading mode (PC1) and the second leading mode (PC2) and the solar irradiance, respectively. Substituting (7) into (8), we get

$$Y(i) = \alpha_0 + \alpha_1\beta_1 T(i) + \alpha_2\beta_2 T(i) + \alpha_3\beta_3 T(i) + \alpha_4\beta_4 T(i) + Y_{noise}(i) \quad (9)$$

$\alpha_1\beta_1, \alpha_2\beta_2, \alpha_3\beta_3, \alpha_4\beta_4$ represent the contribution of the four independent variables to the trend of the climate variable, which can be simply expressed by the following equation:

$$Y_{trend}(i) = \alpha_1 X_{trend1}(i) + \alpha_2 X_{trend2}(i) + \alpha_3 X_{trend3}(i) + \alpha_4 X_{trend4}(i) \quad (10)$$

Student's t-test assesses the statistical significance of the trends in this study.

3. The relationship between SSW trends and tropical Pacific convection enhancement

Fig. 1 shows the time series of the duration and strength of SSWs in winter. It can be seen from the NCEP data that although SSWs have a large inter-annual variability, during the period of 1948-2003, the increasing trend of SSW duration and the increasing trend of SSW strength are statistically significant above 95% confidence level. But after 2003, the increasing trend of SSW duration and strength did not continue. In the NCEP data, the increase rate of SSW duration is 0.2 day/year and the enhancing rate of SSW strength is 0.004 K/degree/year during 1948-2003. Through another set of data JRA55, it further verified that SSWs had a growing trend before 2003. Since the starting year of JRA55 is 1958, the trend calculation from JRA55 is assigned to 1958-2003. In the JRA55 dataset, the increase rate of SSW duration is 0.14 day/year. The enhancing rate of SSW strength is 0.004 K/degree/year, which are statistically significant at a 95% confidence level. Since there are consistent trends in both datasets, the following research is based on NCEP dataset.

The correlation coefficient between the duration of SSWs and the strength of SSWs is 0.7, implies the winter with longer SSWs is tend to have stronger SSWs. This can be explained by the study of the single SSW events, which shows that the SSW is more likely to have greater strength when it lasts long (Li and Tian 2017). The consistent variations of the SSW duration and SSW strength imply that their trends can be explained by the same impact factors.

Since we calculated the trends of different starting times, the trends of SSW during 1948-2003 and 1958-2003 are both statistically significant, so it can be estimated that the selection of different starting times to calculate the trends of SSW will not have an

important influence on the results of the analysis. Since the trend of SSW has undergone significant changes around 2003, the determination of the turning point has become a very important issue. Due to the inter-annual variability of SSW is very huge, no matter what statistical method is adopted, the selection of the turning point cannot be very accurate, and only qualitative analysis can be done. For NCEP data, we set 1948 as the starting point, and select different endpoints to calculate and compare the trends. Fig. 2b shows the trends of SSW duration correspond to different years selected as endpoints. If 2003 is chosen as the turning point of the SSW duration, the trend of SSW duration before this year reaches the maximum. If the years after 2003 is chosen to calculate the trend of SSW duration, the value of the increasing trend is getting smaller. This is because, after 2003, the trend of SSW duration no longer exists, and if these years are used as endpoints, the trend of SSW is even less obvious. For JRA55 data, we set 1958 as the starting point, the result is almost the same as the result in NCEP. Fig. 2c discusses the trends of SSW strength calculating by selecting different endpoints. Although the selection of 2003 as the turning point cannot make the trend of SSW strength reach the maximum, it can be seen that if the year after 2003 is selected to calculate the trend of SSW strength, the trend of SSW strength becomes no longer significant. Choosing 2003 as the turning point to analyze the SSW trend and explore the influencing factors has more physical meaning, which can be seen from the following analysis of the cloudiness time series.

Fig. 3a shows the trends of cloudiness in the tropical Pacific region during 1948-2017, which implies the convective activities in the box region of 170°W - 110°W, 18°S

-3°N has increased significantly. Deser (2010) found an eastward extension of atmospheric deep convection from the Maritime Continent to the central equatorial Pacific. The pattern of enhanced convective activities given by Deser (2010) is similar to the pattern of increased cloudiness in the Fig. 3a. Fig 3b shows the interannual variation of the winter-mean cloudiness averaged in the box region. During the period of 1948-2003, the enhancement trend of cloudiness is statistically significant above 99% confidence level, and around 2003, the trend of enhancing convection ceased. The trend of the winter-mean cloudiness during 1948-2003 is 0. 13 okta/10 yr. Same as the analysis method applied in exploring the turning point of the SSW trend, we explore the turning point of the trend of cloudiness, and the result is shown in Fig. 2a. Since the inter-annual variability of cloudiness is much smaller than that of SSW, the curve in Fig. 2a is smoother and reliable. If the year around 2003 is chosen as the turning point, the trend of cloudiness before the turning point would reach the maximum. The curve in Fig. 2a is similar to that in Fig. 2b, which implies that there is a certain physical mechanism connection between cloudiness and the duration of SSWs.

In this study, we adopt cloudiness to measure the convective activities. Whether the cloudiness is capable of representing the convective activities in the tropical Pacific is assessed. Fig. 4a shows the patterns of the climatological mean of the cloudiness and precipitation averaged for 1979-2017, since GPCP Version 2.3 Combined Precipitation Data Set is only available after 1979. Fig. 4a shows that the climatological pattern of cloudiness is consistent with that of precipitation. Fig. 4b shows not only the climatology mean, but also in the interannual time scale, the cloudiness and

precipitation have a proportional relationship. Thus, the cloudiness can replace the precipitation to indicate the convective activities in the box region. Winter tropical convective anomalies can release a large amount of latent heat energy, heat the atmosphere around, which would furtherly modulate circulations outside tropics (Wang et al. 2016; Guo et al. 2017). Fig. 4b also shows the scatter plot of the winter-mean cloudiness and the tropospheric heat source in the box region. The heating of the atmosphere is proportional to the intensity of convective activities in the box region. When the cloudiness in the box region is above (below) 4.5 okta, the values of tropospheric heat source are above (below) zero, which means the troposphere in the box region is a heat source (sink).

The box region is the minimum area of the climatic cloudiness. Convective activities in the box area are surrounded by the intertropical convergence zone (ITCZ) and the South Pacific convergence zone (SPCZ), forming a lower area of convective activities. However, the relative change in cloudiness is the largest in the whole tropical Pacific area. The change of cloudiness in the box region during 1948-2003 can reach approximately 20% of the amount of climatological mean (Fig. 4c).

In order to estimate to what extent, the enhancement of convective activities affects the trends of the duration and the strength of SSWs, a multiple regression model is adopted to reconstruct the trends of SSW duration and SSW strength and estimate the contribution of enhancement of the convective activities to the SSW trends. Since previous studies have mentioned that ENSO (e.g., Garfinkel and Hartmann, 2008; Bell et al. 2009; Ren et al. 2011), the extratropical SST anomalies (Jadin et al. 2010; Woo

et al. 2015; Li et al. 2018) and solar variability (Shindell et al. 1999) would modulate SSWs. It is suitable to use a multiple linear regression model after verifying whether these factors are independent of each other. The time series of cloudiness is independent of PC1, PC2 and solar irradiance. If the indices of Niño 3.4 (https://www.esrl.noaa.gov/psd/data/climateindices/list/) is used to represent ENSO, then the correlation coefficient of cloudiness and Niño 3.4 is 0.5. This shows that the cloudiness in the box region has a relation with ENSO on the interannual scale. It is not possible to put the ENSO index and cloudiness into the multiple regression model at the same time. Further analysis found Niño 3.4 doesn't have a significant trend during 1948-2003 (the slope of Niño 3.4 is about 0.01 °C/yr), according to Eq. (9), the contribution of ENSO to the trend of SSW is not significant. Thus, cloudiness, rather than Niño 3.4 is used in the multiple regression model. It should be emphasized that not using Niño 3.4 in the regression model is only suitable for the study of trends. From the perspective of inter-annual changes, the impact of ENSO on SSWs is significant and should not be ignored.

After cloudiness, PC1, PC2, and solar irradiance are included in the multiple linear regression model as independent variables, and the contributions of convective activities and other factors on the trends of SSWs are shown in Fig. 5. The majority of the trends in the duration and strength of SSW can be obtained from the enhancement of convective activities in the box region. The contributions of the extratropical SST signals and solar activities to the SSW trends are negligible. In this research, we would focus on how the enhancement of convective activities in the box region affects the

346 trends of the duration and strength of SSWs.

347

348 4. **Mechanism of the convective activity enhancement modulating SSW trends**

349 **a. Impacts of convective activities on teleconnections**

350 Fig. 6a shows the patterns of 200 hPa geopotential height and winds regressed on
351 the standardized winter cloudiness in the box region. A north-south symmetrical
352 anticyclonic structure appears in the tropical Central Pacific, which is triggered by
353 tropical convective activities. According to previous works such as Hoskins et al. (1977)
354 and Gill, (1980), the vorticity perturbations would propagate along the spherical surface
355 to mid-high latitudes. The correlation coefficient between winter-mean PNA and
356 cloudiness is 0.52. The correlation coefficient between winter-mean WP and cloudiness
357 is 0.42. The spatial correlation coefficient between the patterns of PNA (WP) and
358 extratropical geopotential anomalies induced by convective activities is 0.7 (0.6), which
359 illustrated the enhancement of the convective activities in the box region would induce
360 a wave train similar to PNA and WP.

361 Fig. 6b shows the patterns of 200 hPa geopotential height regressed on the
362 standardized time series of SSW duration in Fig. 1a. At middle and high latitudes, there
363 exist negative geopotential height anomalies over North Pacific to Siberia and positive
364 height anomalies over Canada. In the winter of more SSWs, there are significant
365 positive anomalies in the geopotential height field in the tropical Pacific, which is
366 closely related to the enhancement of convective activities. The spatial correlation
367 coefficient between the geopotential height field regressed on the cloudiness and that

368 regressed on SSW duration is 0.8. Comparing Fig. 6a and Fig. 6b, both from the
369 perspectives of pattern and magnitude, the height anomalies associated with SSWs
370 resemble the anomalies caused by the enhancement of convective activities. The first
371 step for the convective activities to adjust the trend of SSW is to stimulate wave trains
372 like PNA and WP to form geopotential height anomalies in the middle and high latitudes
373 that are conducive to SSW.
374
375 **b. Impacts of convective activities on the extratropical planetary waves**
376 Since the stratosphere can only allow large-scale planetary waves to propagate to
377 the stratosphere, SSWs are mainly regulated by the break of these planetary waves. Fig.
378 7 shows how the enhancement of convective activities impacts PW1 and PW2. When
379 the convective activities are active in the box region of Fig. 3a, the trough of PW1
380 aroused by convective activities is located from Siberia to Aleutian Islands, and the
381 crest of PW1 is located from Northeast Canada to North Atlantic (Fig. 7a). The trough
382 of PW1 of climatology is also located from Siberia to North Pacific, and the crest of
383 PW1 of climatology is located from Northeast Canada to North Atlantic. The difference
384 is that the climatological crest and trough are more southerly. Since PW1 anomalies
385 aroused by the enhanced convective activities in the box region coincide with the
386 climatological pattern, PW1 in the troposphere is enhanced.
387 Fig. 7b shows the relationship between PW2 anomalies caused by convective
388 enhancement and the climatological pattern of PW2. The troughs of PW2 of
389 climatology are located in Hudson Bay in Canada and Siberia, and the crests of PW2

are located in Northern Europe and Alaska. The troughs of PW2 aroused by convective activities are located in Sakhalin and North Atlantic, and the crests of PW2 are located in Northern America and Northern Asia. Since the anomalies of PW2 are 90° out of phase with the climatological PW2 and the amplitude of the anomalies of PW2 is small, the changes of PW2 caused by convective enhancement are not significant. While the changes of PW1 caused by convective enhancement are significant and occupy the main component in the large-scale planetary wave changes.

Fig. 8 shows the time series of 100 hPa vertical component of EP flux averaged from 45°N to 90°N. It can be seen that during the period of 1948-2003, the increasing trend of PW1 in mid-to-high latitudes is statistically significant above 99% confidence level. But after 2003, PW1 shows a decreasing trend. The increasing rate of PW1 is 800 m^3s^{-2}/year during 1948-2003. PW2 in mid-to-high latitudes did not increase during 1948-2003, while there have been large abnormalities in several years after 2003. It can be seen by comparing with Fig. 3b that the trend changes in the convective activities in the box region and those of PW1 in mid-to-high latitudes are highly synchronized. The trends of PW2 and convective activities are not synchronized. This is because of the reasons explained in Fig. 7, that PW1 anomalies aroused by the enhanced convective activities in the box region coincide with the climatological pattern, but PW2 anomalies don't. In addition, the strength of PW1 is greater than that of PW2, thus PW1 plays a greater role in affecting the trend change of SSW.

Fig. 8 illustrates the change of large-scale planetary waves at mid-high latitudes in the tropopause, and Fig. 9 illustrates the change of planetary waves at mid-high latitudes

412 in the stratosphere. The trend of planetary waves in the stratosphere is similar to that in
413 the tropopause. PW1 showed a trend of rising first and then falling around 2003. The
414 change of the trend of PW2 is not significant. Comparing Fig. 8 and Fig. 9, the relative
415 proportions of PW1 and PW2 have changed. In the upper troposphere and lower
416 stratosphere, the intensity of PW1 is 1.7 times that of PW2. In the stratosphere, the
417 intensity of PW1 is 2.8 times that of PW2. This is because the stratosphere has a filtering
418 effect on planetary waves, and planetary waves with a small wavenumber are more
419 penetrating than those with a large wavenumber. Therefore, as the planetary waves are
420 propagated from the troposphere to the stratosphere, the proportion of PW1 in the
421 planetary waves will also increase. It also means that PW1 has a greater impact on SSW
422 than PW2. Therefore, the trend changes of SSW and the trend changes of PW1 in the
423 stratosphere are more consistent.

424 The contributions of convective activities and other independent factors on the
425 trends of PW1 and PW2 in the stratosphere are shown in Fig. 10. The majority of the
426 trend in PW1 during 1948-2003 is contributed from the enhancement of convective
427 activities in the box region. Although the intensity of PW2 also shows an increasing
428 trend during 1948-2003, it is not significant and can be ignored compared with the
429 climatic intensity of PW2.

430 Since the stratosphere is a filter for planetary waves, the conditions of the
431 stratospheric circulation may change the intensity of the planetary waves reaching the
432 stratosphere, thereby affecting the trend of planetary waves. In order to qualitatively
433 estimate the change of the planetary wave transmittance rate in the stratosphere, we

calculated the ratio of the intensity of the planetary wave at 20 hPa and 100 hPa. For PW1, the average transmittance rate of the stratosphere is 0.64, and for PW2, the average transmittance rate is 0.44. The transmittance of planetary waves has great interannual changes, but the long-term trend is not significant, so the trend of transmittance rate of PW1 and PW2 is not shown here. According to Eq. (9), under the assumption that the influence of independent variables is linear, this also means that the filtering effect of the stratosphere on planetary waves has no significant influence on the change of SSW trend.

5. **Conclusion and Discussion**

This paper studies the relationship between the trend of convective activities in the tropical central Pacific (box region of 170°W - 110°W, 18°S -3°N) and the trend of SSW from 1948 to 2017. Due to the lack of complete direct observations of convective activities during this period, such as satellite observations of OLR, we used cloudiness observations of International Comprehensive Ocean-Atmosphere Data Set (ICOADS) as a substitute for OLR, and obtained a time series of changes in convective activities in this area from 1948 to 2017. The convection activities in the tropical central Pacific are enhanced during the period of 1948-2003. After 2003, the trend of increased convective activities in the central tropical Pacific did not continue.

By analyzing the planetary waves in the extratropical geopotential height field regressed by the convective activities, we found that the geopotential height anomaly field generated in the mid-high latitudes and the climate state will interact with each

other. The enhanced convective activities in the Central Pacific Ocean make the intensity of PW1 in the extratropical region significantly enhanced, while the impacts on PW2 are not significant. Therefore, PW1 increased during the period of 1948-2003 with the increase of convective activities in the central tropical Pacific. After 2003, the increasing trend was reversed. The change of the trend of PW2 is not obvious, and it is inconsistent with the trend of convective activities.

When the planetary waves in the troposphere are propagated to the stratosphere, the stratosphere has a filtering effect. PW1 with a small wavenumber is passed more and PW2 is blocked more. Thus, in the stratosphere, PW1 occupies a larger proportion in the planetary waves and has a greater impact on SSW.

Through the analysis of NCEP data and JRA55 data, as well as the analysis of the duration and maximum intensity of SSW throughout the winter, we found that SSW had an increasing trend before 2003. Because SSW has large inter-annual variability, it is difficult to use statistical methods to obtain an accurate turning point of the SSW trend. The 2003 year as the turning point is only a qualitative estimate, but it does reflect the characteristics of the SSW trend. Choosing a different start time will not affect the results. This study did not find a significant trend of the frequency of SSW, but the study found that there is a new trend feature in the duration and strength of SSW, which is consistent with the trend of PW1 and the trend of convective activities in the tropical central Pacific. Previous studies on the trend of SSW mostly used frequency as a measurement index, and draw conclusions from this index that there was no significant change in the trend of SSW in the past few decades. This research studies SSW from

478 the perspective of duration and strength, and finds that the trend of SSW has changed,
479 which is the innovation of this article.

480 Through multiple linear regression, we analyzed the contributing factors of this
481 trend and found that compared to the extratropical ocean temperature and solar activity,
482 the increase in convective activities in the central tropical Pacific contributed the most
483 to the trend of SSW. Snow cover and QBO are also important factors to modulate SSWs
484 (Richter et al. 2011). But after the QBO index and snow cover index are added to the
485 regression model, the conclusion does not change. However, there are still many
486 shortcomings in the analysis contribution of the multiple linear regression model. For
487 example, the premise of the use of this model is that the factors are independent of each
488 other, but the atmosphere and ocean systems are nonlinear, and there are deeper
489 interactions between different factors. Future research using a numerical model on this
490 topic is needed.

491 We also use some indexes of ENSO to study the influence of ENSO on the trend
492 of SSW, since these commonly used indexes such as Niño 3.4 did not have a significant
493 trend from 1948 to 2003, it is difficult for ENSO to explain the trend of SSW according
494 to Eq. (9). Nevertheless, we still believe that the enhancement of convective activities
495 in the central tropical Pacific is closely related to ENSO. However, ENSO cannot fully
496 explain the increase in convective activities in the central tropical Pacific, e.g., previous
497 studies claimed the enhancement of convective activities reflected the weakening of the
498 Walker Circulation (e.g., Deser et al. 2010; Tokinaga et al. 2012b). Through the analysis
499 of bucket-sampled SST from ICOADS (Tokinaga, 2012a) and Extended Reconstructed

Sea Surface Temperature (ERSST) version 5, we believe that the enhancement of convective activities in this area is related to the eastward expansion of the equatorial Pacific SST isotherm of 27ºC, which is estimated as the threshold for deep convection. Due to the limited length of the article, this part of the work will be presented in another article.

Acknowledgments

We are grateful to the groups and agencies for providing the datasets used in this study. This work was supported jointly by the National Natural Science Foundation of China (41805029, 41875087, 42030601), and China Postdoctoral Science Foundation (2018M641913).

Reference

Adler RF, Huffman GJ, Chang A, Ferraro R, Xie P-P, Janowiak J, Rudolf B, Schneider U, Curtis S, Bolvin D, Gruber A, Susskind J, Arkin P, Nelkin E (2003) The Version-2 Global Precipitation Climatology Project (GPCP) Monthly Precipitation Analysis (1979–Present). Journal of Hydrometeorology 4:1147-1167.

Andrews DG, Holton JR, Leovy CB (1987) Middle atmosphere dynamics. Academic press, San Diego

Baldwin MP, Dunkerton TJ (1999) Stratospheric harbingers of anomalous weather regimes. Science 294: 581-584.

Baldwin MP, Dunkerton TJ (2001) Propagation of the Arctic Oscillation from the stratosphere to the troposphere. Journal of Geophysical Research: Atmospheres 104: 30937-30946.

Baldwin MP, Coauthors (2021) Sudden Stratospheric Warmings. Reviews of Geophysics 59.

Barnston AG, Livezey RE (1987) Classification, seasonality and persistence of low-frequency atmospheric circulation patterns. Monthly Weather Review 115:1083-1126.

Bell CJ, Gray LJ, Charlton-Perez AJ, Joshi MM, Scaife AA (2009) Stratospheric communication of El Nino teleconnections to European winter. Journal of Climate 22:4083-4096.

Bond NA, Overland JE, Spillane M, Stabeno P (2003) Recent shifts in the state of the North Pacific. Geophysical Research Letters 30.

Broennimann S (2007) Impact of El Nino Southern Oscillation on European climate. Reviews of Geophysics 45.

Butchart N, Austin J, Knight JR, Scaife AA, Gallani ML (2000) The response of the stratospheric climate to projected changes in the concentrations of well-mixed greenhouse gases from 1992 to 2051. Journal of Climate 13:2142-2159.

Butler AH, Seidel DJ, Hardiman SC, Butchart N, Birner T, Match A (2015) Defining sudden stratospheric warmings. Bulletin of the American Meteorological Society 96:1913-1928.

Charlton AJ, Polvani LM (2007) A new look at stratospheric sudden warmings. Part I: Climatology and modeling benchmarks. Journal of Climate 20:449-469.

Davini P, Cagnazzo C, Anstey JA (2014) A blocking view of the stratosphere-troposphere coupling. Journal of Geophysical Research-Atmospheres 119:11100-11115.

542 Deser C, Phillips AS, Alexander MA (2010) Twentieth century tropical sea surface temperature
543 trends revisited. Geophysical Research Letters 37.
544 Ding Y (1989) Diagnostic and analytical methods in synoptic dynamics. Science Press, Beijing.
545 Domeisen DIV (2019) Estimating the Frequency of Sudden Stratospheric Warming Events From
546 Surface Observations of the North Atlantic Oscillation. Journal of Geophysical Research-
547 Atmospheres 124:3180-3194.
548 Garfinkel CI, Hartmann DL (2008) Different ENSO teleconnections and their effects on the
549 stratospheric polar vortex. Journal of Geophysical Research-Atmospheres 113.
550 Garfinkel CI, Schwartz C (2017) MJO-Related Tropical Convection Anomalies Lead to More
551 Accurate Stratospheric Vortex Variability in Subseasonal Forecast Models. Geophysical Research
552 Letters 44:10054-10062.
553 Gill AE (1980) Some simple solutions for heat-induced tropical circulation. Quarterly Journal of
554 the Royal Meteorological Society 106:447-462.
555 Guo Y, Ting M, Wen Z, Lee DE (2017) Distinct patterns of tropical Pacific SST anomaly and their
556 impacts on North American climate. Journal of Climate 30:5221-5241.
557 Harada Y, Kamahori H, Kobayashi C, Endo H, Kobayashi S, Ota Y, Onoda H, Onogi K, Miyaoka
558 K, Takahashi K (2016) The JRA-55 Reanalysis: Representation of Atmospheric Circulation and
559 Climate Variability. Journal of the Meteorological Society of Japan 94:269-302.
560 Hendon HH (2019) Rare climate event was forecast. Nature 573:495-495.
561 Holton JR (1976) A semi-spectral numerical model for wave-mean flow interactions in the
562 stratosphere: Application to sudden stratospheric warmings. Journal of the Atmospheric Sciences
563 33:1639-1649.
564 Horel JD, Wallace JM (1981) Planetary-scale atmospheric phenomena associated with the
565 Southern Oscillation. Monthly Weather Review 109:813-829.
566 Hoskins BJ, Simmons AJ, Andrews DG (1977) Energy dispersion in a barotropic atmosphere.
567 Quarterly Journal of the Royal Meteorological Society 103:553-567.
568 Hu D, Guan Z, Tian W, Ren R (2018) Recent strengthening of the stratospheric Arctic vortex
569 response to warming in the central North Pacific. Nature Communications 9.
570 Jadin EA, Wei K, Zyulyaeva YA, Chen W, Wang L (2010) Stratospheric wave activity and the
571 Pacific Decadal Oscillation. Journal of Atmospheric and Solar-Terrestrial Physics 72:1163-1170.

572 Kalnay E, Kanamitsu M, Kistler R, Collins W, Deaven D, Gandin L, Iredell M, Saha S, White G,
573 Woollen J, Zhu Y, Chelliah M, Ebisuzaki W, Higgins W, Janowiak J, Mo KC, Ropelewski C,
574 Wang J, Leetmaa A, Reynolds R, Jenne R, Joseph D (1996) The NCEP/NCAR 40-year reanalysis
575 project. Bulletin of the American Meteorological Society 77:437-471.
576 Kobayashi S, Ota Y, Harada Y, Ebita A, Moriya M, Onoda H, Onogi K, Kamahori H, Kobayashi
577 C, Endo H, Miyaoka K, Takahashi K (2015) The JRA-55 Reanalysis: General Specifications and
578 Basic Characteristics. Journal of the Meteorological Society of Japan 93:5-48.
579 Kodera K (1991) The solar and equatorial QBO influences on the stratospheric circulation during
580 the early northern-hemisphere winter. Geophysical Research Letters 18:1023-1026.
581 Kolstad EW, Breiteig T, Scaife AA (2010) The association between stratospheric weak polar
582 vortex events and cold air outbreaks in the Northern Hemisphere. Quarterly Journal of the Royal
583 Meteorological Society 136:886-893.
584 Kuroda Y, Kodera K (2002) Effect of solar activity on the Polar-night jet oscillation in the
585 northern and southern hemisphere winter. Journal of the Meteorological Society of Japan 80:973-
586 984.
587 Li Y, Tian W (2017) Different impact of central Pacific and eastern Pacific El Niño on the duration
588 of sudden stratospheric warming. Advances in Atmospheric Sciences 34:771-782.
589 Li Y, Tian W, Xie F, Wen Z, Zhang J, Hu D, Han Y (2018) The connection between the second
590 leading mode of the winter North Pacific sea surface temperature anomalies and stratospheric
591 sudden warming events. Climate Dynamics 51:581-595.
592 Lim E-P, Hendon HH, Boschat G, Hudson D, Thompson DWJ, Dowdy AJ, Arblaster JM (2019)
593 Australian hot and dry extremes induced by weakenings of the stratospheric polar vortex. Nature
594 Geoscience 12:896-901.
595 Lu C, Ding Y (2015) Analysis of isentropic potential vorticities for the relationship between
596 stratospheric anomalies and the cooling process in China. Science Bulletin 60:726-738.
597 Lukens KE, Feldstein SB, Yoo C, Lee S (2017) The dynamics of the extratropical response to
598 Madden-Julian Oscillation convection. Quarterly Journal of the Royal Meteorological Society
599 143:1095-1106.

600 Mantua NJ, Hare SR, Zhang Y, Wallace JM, Francis RC (1997) A Pacific interdecadal climate
601 oscillation with impacts on salmon production. Bulletin of the American Meteorological Society
602 78:1069-1079.
603 Matsuno T (1970) Vertical propagation of stationary planetary waves in the winter Northern
604 Hemisphere. Journal of the atmospheric sciences, 27, 871-883.
605 Matsuno T (1971) A dynamical model of the stratospheric sudden warming. Journal of the
606 Atmospheric Sciences, 28, 1479-1494.
607 Mitchell DM, Gray LJ, Anstey J, Baldwin MP, Charlton-Perez AJ (2013) The Influence of
608 Stratospheric Vortex Displacements and Splits on Surface Climate. Journal of Climate 26:2668-
609 2682.
610 Mudelsee M (2019) Trend analysis of climate time series: A review of methods. Earth-Science
611 Reviews 190:310-322.
612 Quiroz RS (1977) The tropospheric-stratospheric polar vortex breakdown of January 1977.
613 Geophysical Research Letters 4:151-154.
614 Rao J, Garfinkel CI, White IP, Schwartz C (2020) The Southern Hemisphere Minor Sudden
615 Stratospheric Warming in September 2019 and its Predictions in S2S Models. Journal of
616 Geophysical Research-Atmospheres 125.
617 Reichler T, Kim J, Manzini E, Kroeger J (2012) A stratospheric connection to Atlantic climate
618 variability. Nature Geoscience 5:783-787.
619 Richter JH, Matthes K, Calvo N, Gray (2011) Influence of the quasi-biennial oscillation and El
620 Nino–Southern Oscillation on the frequency of sudden stratospheric warmings. Journal of
621 Geophysical Research: Atmospheres 116.
622 Schimanke S, Spangehl T, Huebener H, Cubasch U (2013) Variability and trends of major
623 stratospheric warmings in simulations under constant and increasing GHG concentrations. Climate
624 Dynamics 40:1733-1747.
625 Seo K-H, Son S-W (2012) The Global Atmospheric Circulation Response to Tropical Diabatic
626 Heating Associated with the Madden-Julian Oscillation during Northern Winter. Journal of the
627 Atmospheric Sciences 69:79-96.
628 Shindell D, Rind D, Balachandran N, Lean J, Lonergan P (1999) Solar cycle variability, ozone,
629 and climate. Science 284:305-308.

630 Thompson DWJ, Wallace JM (2001) Regional climate impacts of the Northern Hemisphere
631 annular mode. Science 293:85-89.
632 Tokinaga H, Xie S-P, Deser C, Kosaka Y, Okumura YM (2012a) Slowdown of the Walker
633 circulation driven by tropical Indo-Pacific warming. Nature 491:439-443.
634 Tokinaga H, Xie S-P, Timmermann A, McGregor S, Ogata T, Kubota H, Okumura YM (2012b)
635 Regional Patterns of Tropical Indo-Pacific Climate Change: Evidence of the Walker Circulation
636 Weakening. Journal of Climate 25:1689-1710.
637 Wang J, Wen Z, Wu R, Guo Y, Chen Z (2016) The mechanism of growth of the low-frequency
638 East Asia-Pacific teleconnection and the triggering role of tropical intraseasonal oscillation.
639 Climate Dynamics 46:3965-3977.
640 Wang L, Chen W (2010) Downward Arctic Oscillation signal associated with moderate weak
641 stratospheric polar vortex and the cold December 2009. Geophysical Research Letters 37.
642 Wang SYS, Lin Y-H, Lee M-Y, Yoon J-H, Meyer JDD, Rasch PJ (2017) Accelerated increase in
643 the Arctic tropospheric warming events surpassing stratospheric warming events during winter.
644 Geophysical Research Letters 44:3806-3815.
645 Waugh DW, Sobel AH, Polvani LM (2017) What is the polar vortex and how does it influence
646 weather? Bulletin of the American Meteorological Society 98:37-44.
647 WMO/IQSY (1964) International years of the Quiet Sun (IQSY) 1964-65. Alert messages with
648 special references to stratwarms. WMO/IQSY Report No 6, Secretariat of the World
649 Meteorological Organization, Geneva, Switzerland. World Meteorological Organization.
650 Woo S-H, Sung M-K, Son S-W, Kug J-S (2015) Connection between weak stratospheric vortex
651 events and the Pacific Decadal Oscillation. Climate Dynamics 45:3481-3492.
652 Woodruff SD, Worley SJ, Lubker SJ, Ji Z, Freeman JE, Berry DI, Brohan P, Kent EC, Reynolds
653 RW, Smith SR, Wilkinson C (2011) ICOADS Release 2.5: extensions and enhancements to the
654 surface marine meteorological archive. International Journal of Climatology 31:951-967.
655 Zhang J, Tian W, Wang Z, Xie F, Wang F (2015) The influence of ENSO on Northern midlatitude
656 Ozone during the winter to spring transition. Journal of Climate 28:4774-4793.
657 Zhou Z-Q, Xie S-P, Zheng X-T, Liu Q, Wang H (2014) Global Warming-Induced Changes in El
658 Nino Teleconnections over the North Pacific and North America. Journal of Climate 27:9050-
659 9064.

Figures

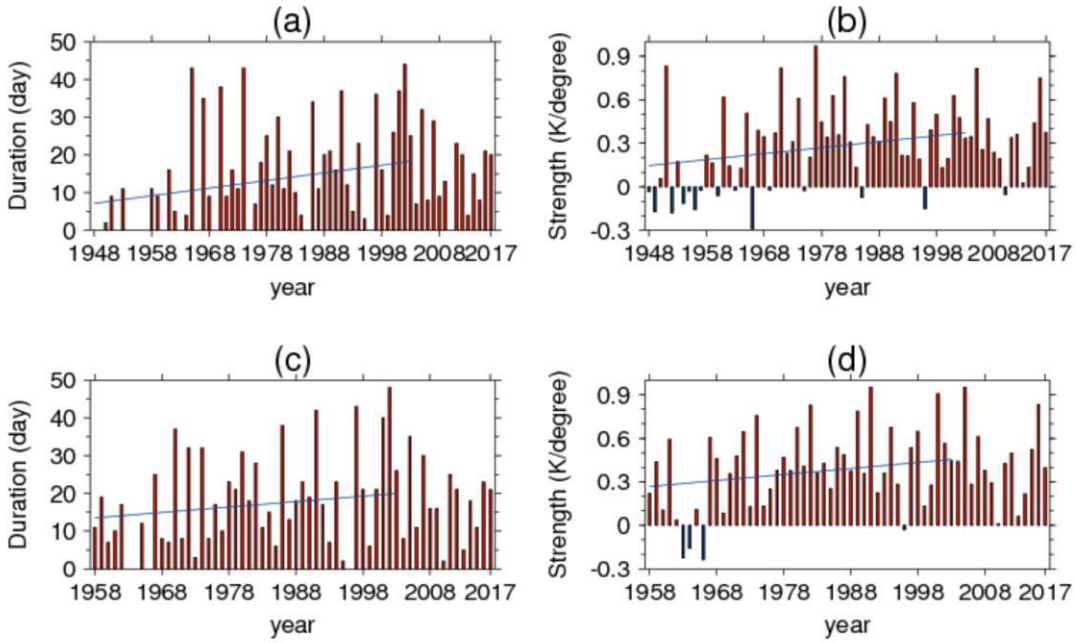

Fig. 1 Time series of (a) SSW duration (unit: days) and (b) SSW strength (unit: K/ degree) in winter (DJF) from 1948 to 2017 derived from NCEP. (c) SSW duration and (d) SSW strength in winter from 1958 to 2017 derived from JRA55. The blue lines in the top two graphs illustrate the linear trends between 1948 to 2003, while those in the bottom two graphs illustrate the linear trends between 1958 to 2003

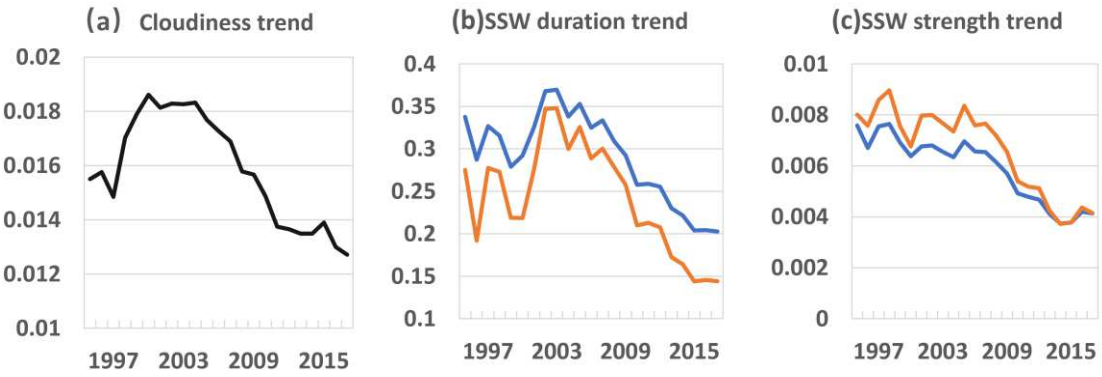

669

670 **Fig. 2** The trends of (a) cloudiness (unit: okta/yr), (b) SSW duration (unit: day/yr),

671 and (c) SSW strength (unit: K/ degree /yr) calculated from a fixed start point to

672 different endpoint. The years in the abscissa correspond to the different endpoint. The

673 black line in (a) is calculated from the time series in Fig. 3b with 1948 fixed as the

674 start point. The blue line in (b) and (c) is calculated from the time series of Fig. 1a and

675 Fig. 1b with 1948 fixed as the start point, and the orange line is calculated from the

676 time series of Fig. 1c and Fig. 1d with 1958 fixed as the start point

677

678

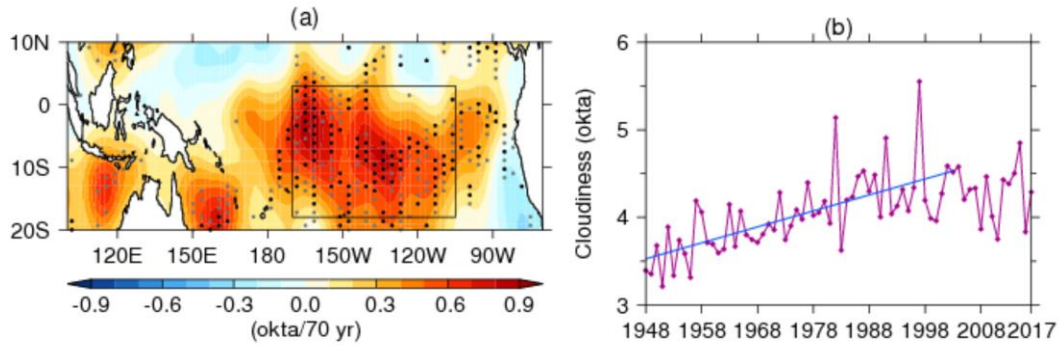

679

680 **Fig. 3** (a) Trends of winter cloudiness in the tropical Pacific region for 1948–2003

681 (unit: okta/55 yr). The trends over the black dotted regions are statistically significant

682 at 95% confidence level. The range of the box is [170°W - 110°W, 18°S -3°N]. (b)

683 Time series of winter cloudiness of the box region (unit: okta) and its trend. The

684 cloudiness is observed data from ICOADS

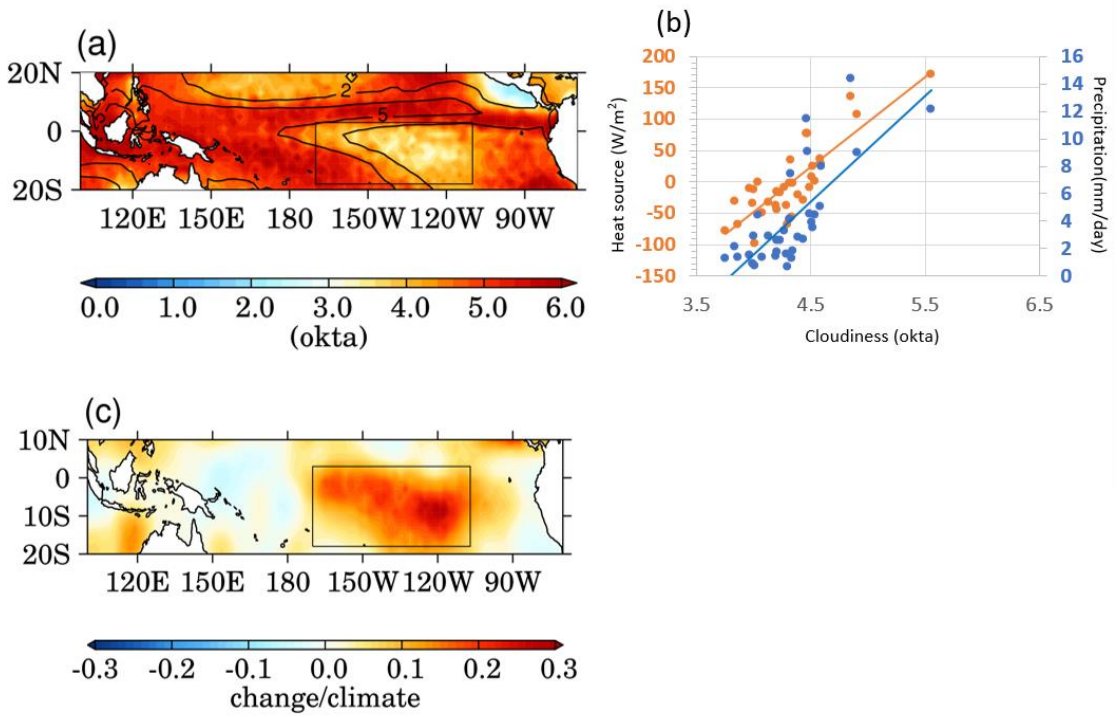

Fig. 4 (a) Climatological winter cloudiness (unit: okta) (color shadings) and precipitation rate (unit: mm day^{-1}) (contour). The precipitation data is derived from GPCP Version 2.3 Combined Precipitation Data Set for 1979-2017. (b) The scatter diagram of the winter cloudiness vs. precipitation rate (blue dots) and winter cloudiness vs. tropospheric heat source Q1 (unit: W/m^2, orange dots). The tropospheric heat source is integrated from 1000 hPa to 100 hPa over the box region using Eq. (2). (c) The ratio of the increment of cloudiness during 1948-2003 and the climatology mean

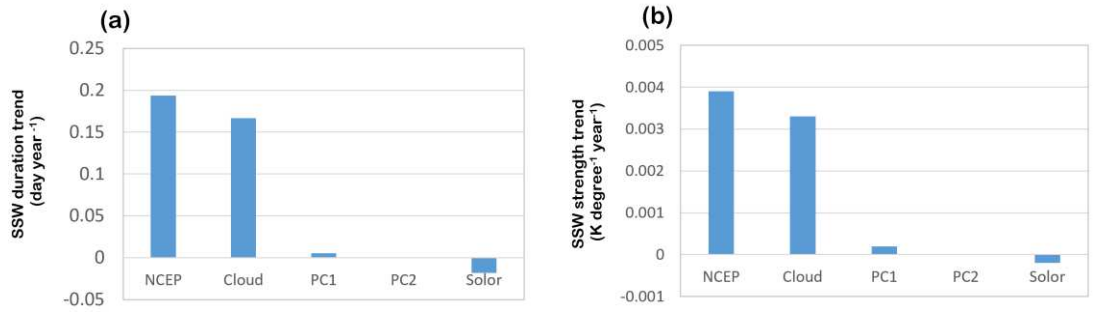

Fig. 5 Contributions of different independent variables on the trends of (a) SSW duration (unit: day/yr) and (b) SSW strength (unit: K/ degree /yr). The trends are calculated in the period of 1948-2003. A multiple regression model adopted to calculate contribution is illustrated in the method section

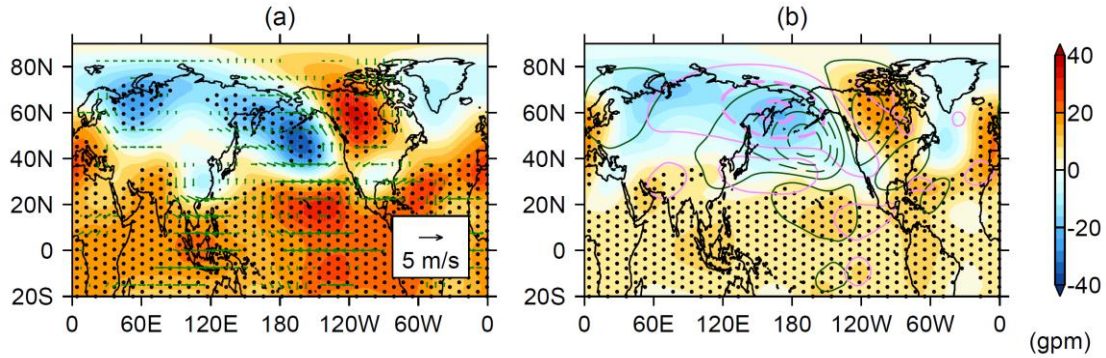

706

707 **Fig. 6** (a) Patterns of 200 hPa geopotential height (unit: gpm; color shadings) and winds

708 (unit: m s^{-1}; vectors) regressed on the standardized winter cloudiness in Fig. 3b. (b)

709 Patterns of 200 hPa geopotential height regressed on the standardized SSW duration

710 index in Fig. 1a. The contours in pink and green colors are representing the patterns of

711 geopotential height anomalies regressed on WP and PNA teleconnections, in which the

712 intervals are 20 gpm. The regions of dots exceed 99% confidence level

713

714

715

716

717

718

719

720

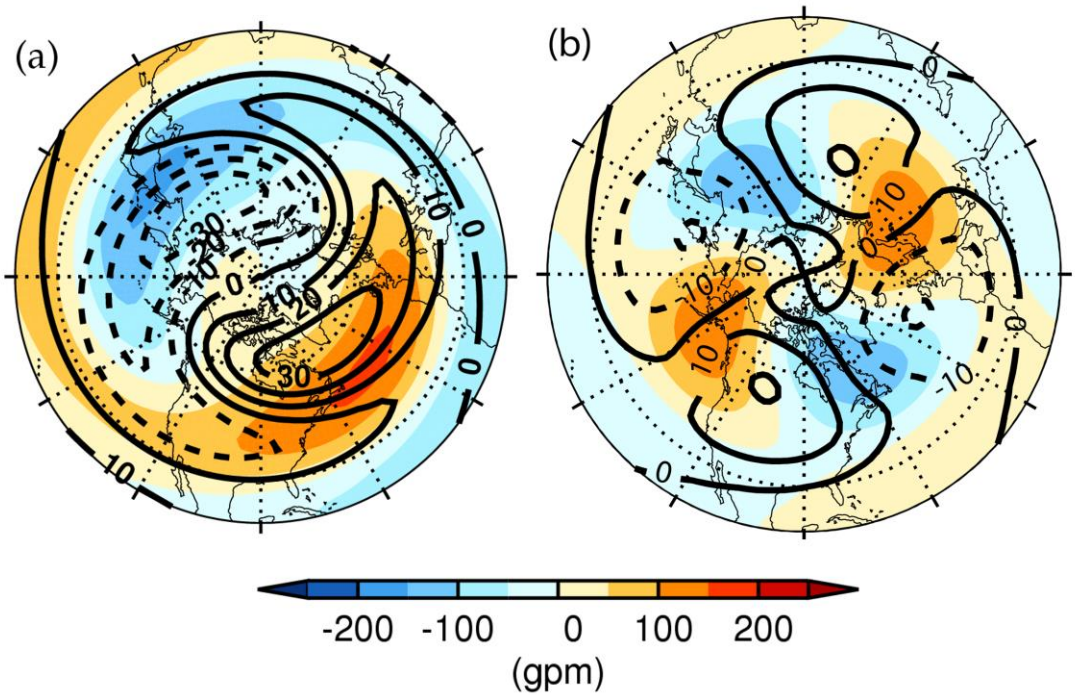

721

722 **Fig. 7** (a) planetary wave 1 (PW1) and (b) planetary wave 2 (PW2) components of the

723 regressed geopotential height field in Fig. 6a. Black contour lines with the intervals of

724 ± 10, ± 20, ± 30 gpm. The color-filled contours show the climatological pattern of

725 PW1 and PW2

726

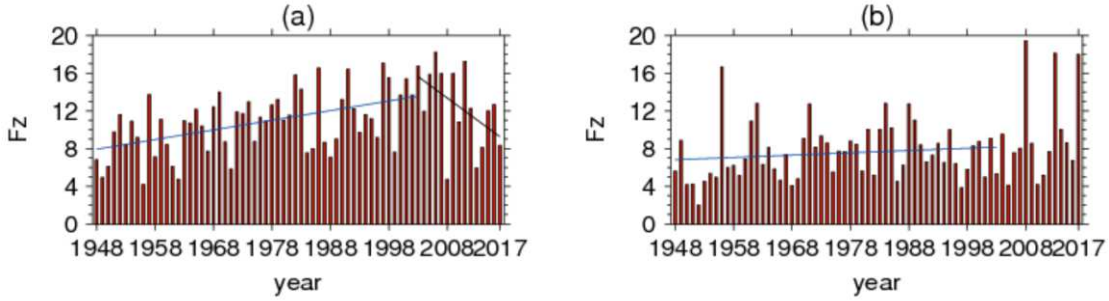

Fig. 8 The time series of the winter $F^{(z)}$ (unit: $10^4 m^3 s^{-2}$) at 100 hPa over the latitude band of 45°N–90°N associated with (a) PW1 and (b) PW2 components derived from the NCEP/NCAR reanalysis data. The blue line is the trend line from 1948 to 2003, and the black line is the trend line from 2004 to 2017

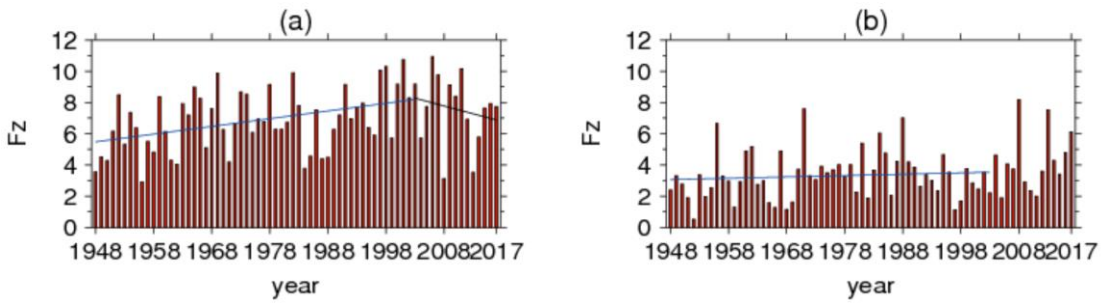

Fig. 9 The time series of the winter $F^{(z)}$ (unit: $10^4 m^3 s^{-2}$) at 20 hPa over the latitude band of 45°N–90°N associated with (a) PW1 and (b) PW2 components derived from the NCEP/NCAR reanalysis data. The blue line is the trend line from 1948 to 2003, and the black line is the trend line from 2004 to 2017

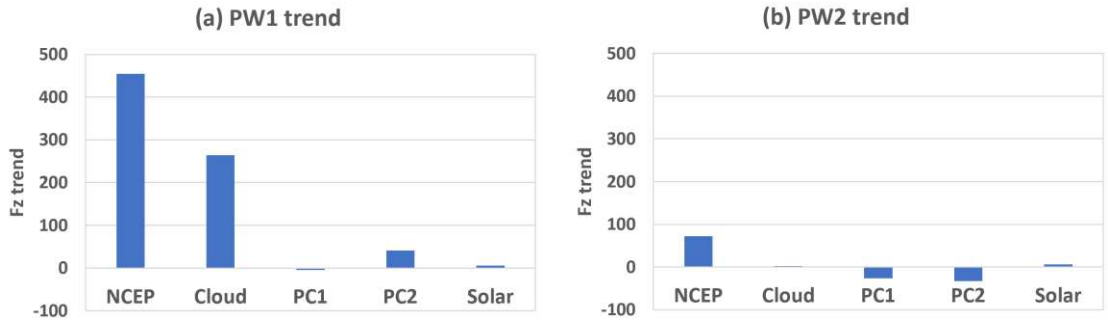

Fig. 10 Contributions (unit: m^3s^{-2}/year) of different independent variables on the trends of (a) PW1 and (b) PW2 at 20 hPa. The trends are calculated in the period of 1948-2003. The independent variables are the same as in Fig. 5

Figures

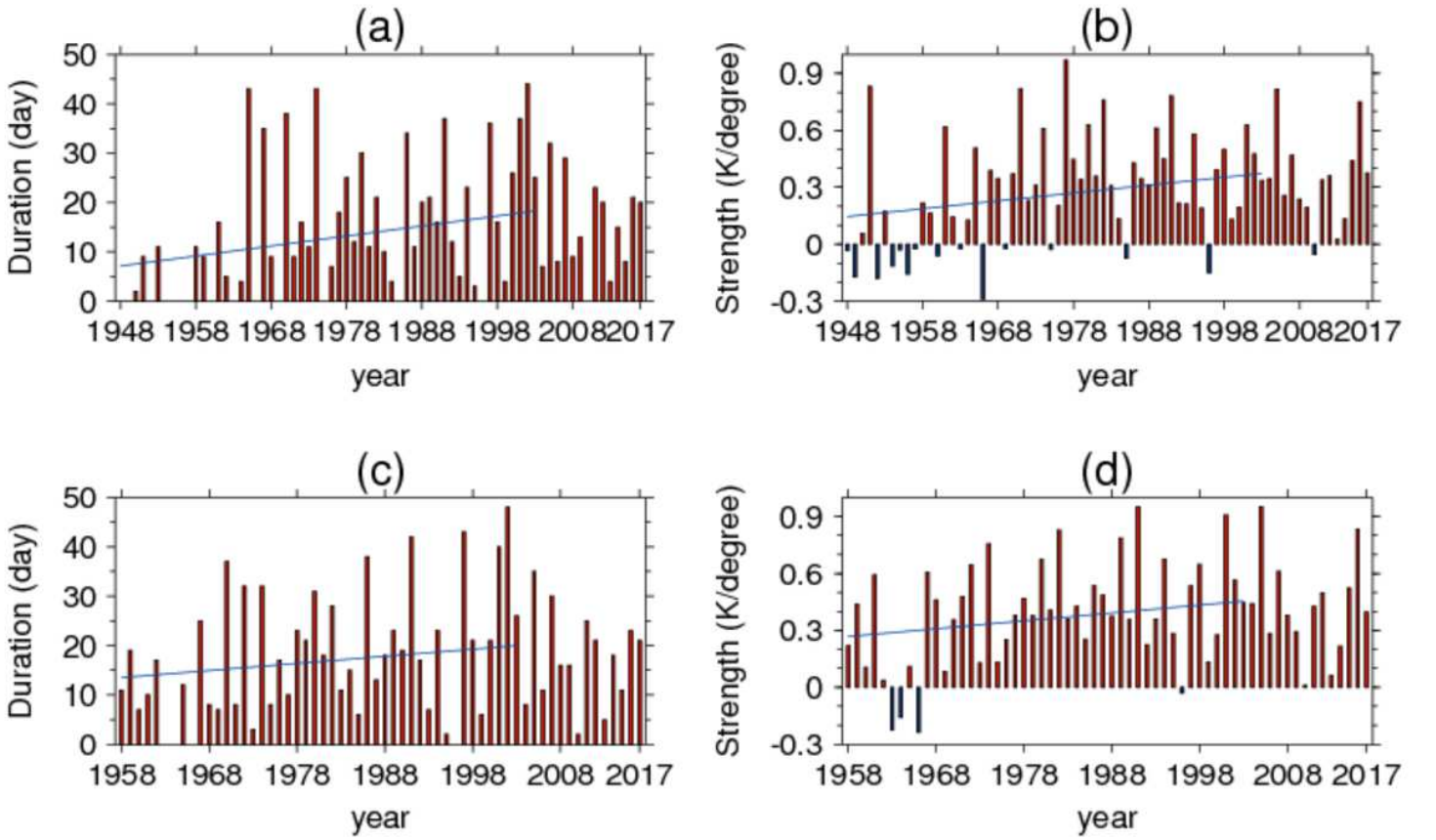

Figure 1

Time series of (a) SSW duration (unit: days) and (b) SSW strength (unit: K/ degree) in winter (DJF) from 1948 to 2017 derived from NCEP. (c) SSW duration and (d) SSW strength in winter from 1958 to 2017 derived from JRA55. The blue lines in the top two graphs illustrate the linear trends between 1948 to 2003, while those in the bottom two graphs illustrate the linear trends between 1958 to 2003

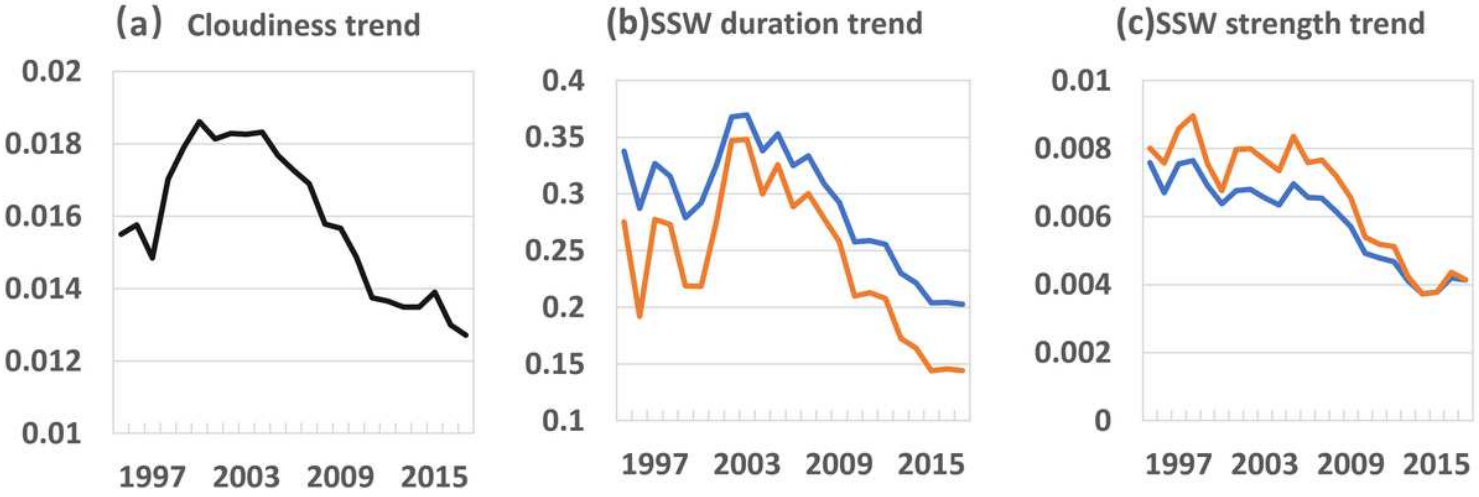

Figure 2

The trends of (a) cloudiness (unit: okta/yr), (b) SSW duration (unit: day/yr), and (c) SSW strength (unit: K/ degree /yr) calculated from a fixed start point to different endpoint. The years in the abscissa correspond to the different endpoint. The black line in (a) is calculated from the time series in Fig. 3b with 1948 fixed as the start point. The blue line in (b) and (c) is calculated from the time series of Fig. 1a and Fig. 1b with 1948 fixed as the start point, and the orange line is calculated from the time series of Fig. 1c and Fig. 1d with 1958 fixed as the start point

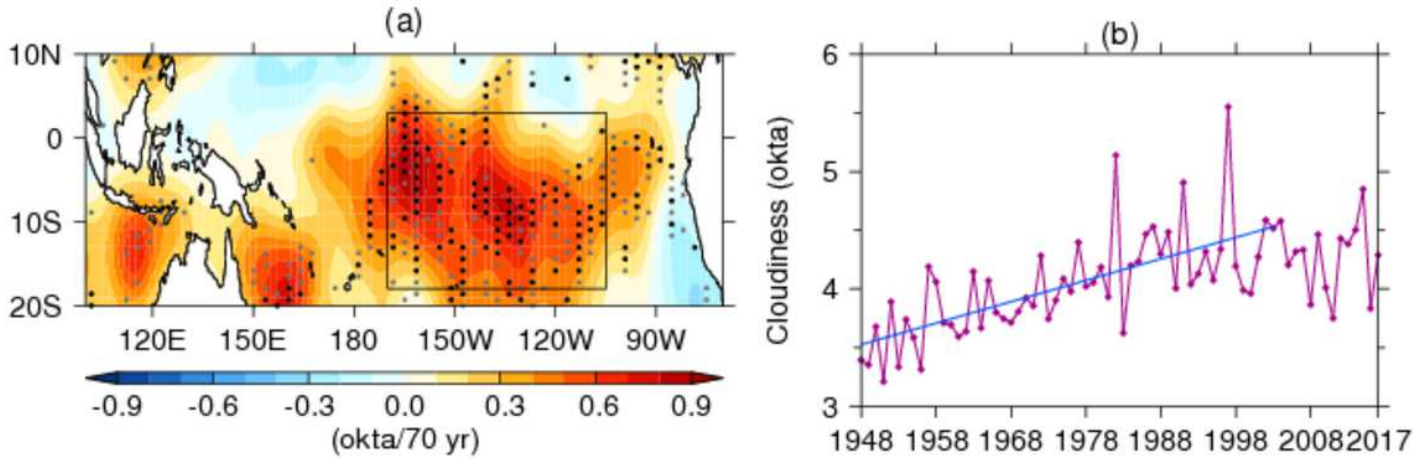

Figure 3

(a) Trends of winter cloudiness in the tropical Pacific region for 1948–2003 (unit: okta/55 yr). The trends over the black dotted regions are statistically significant at 95% confidence level. The range of the box is [170°W - 110°W, 18°S -3°N]. (b) Time series of winter cloudiness of the box region (unit: okta) and its trend. The cloudiness is observed data from ICOADS

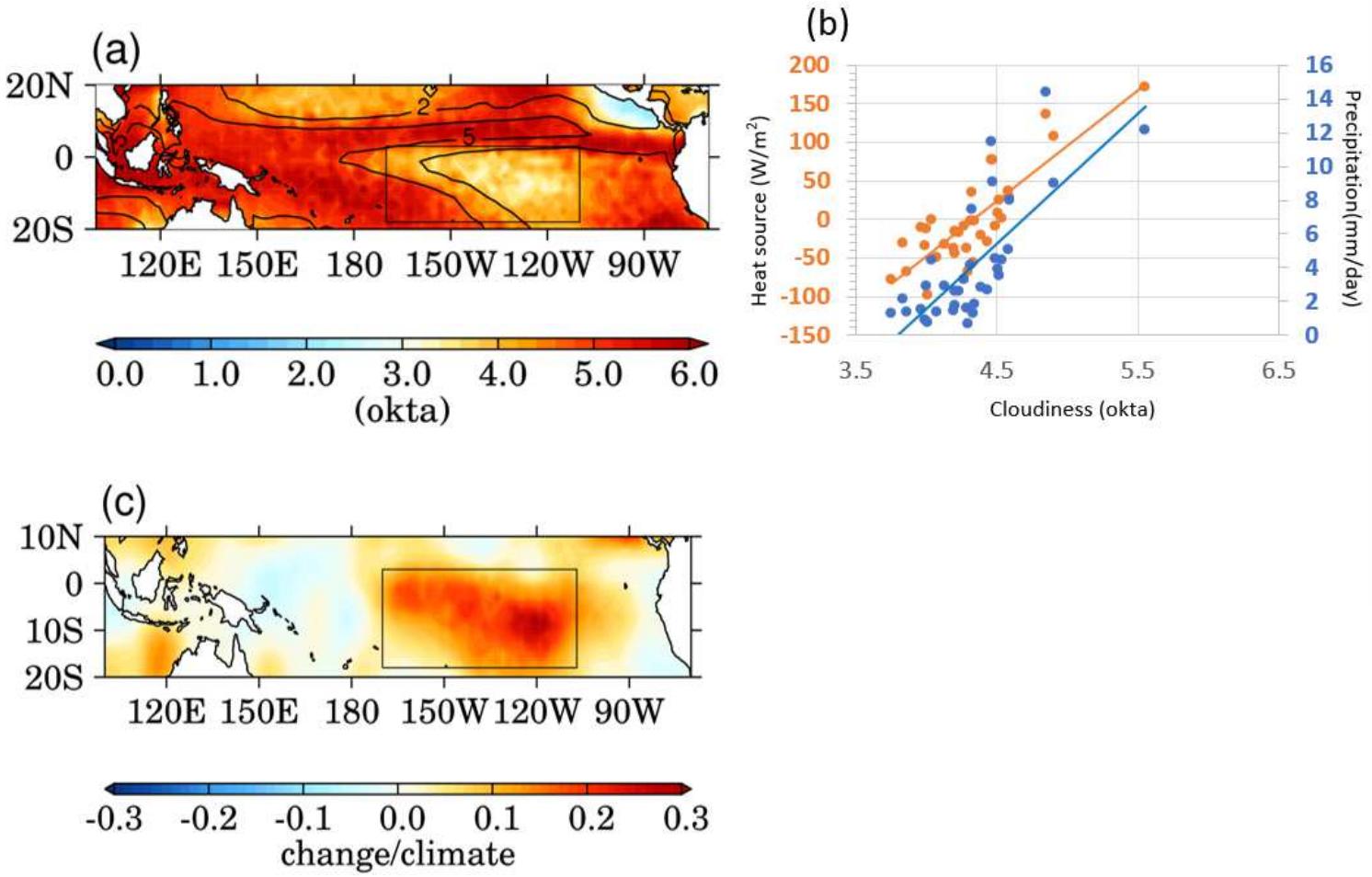

Figure 4

(a) Climatological winter cloudiness (unit: okta) (color shadings) and precipitation rate (unit: mm day-1) (contour). The precipitation data is derived from GPCP Version 2.3 Combined Precipitation Data Set for 1979-2017. (b) The scatter diagram of the winter cloudiness vs. precipitation rate (blue dots) and winter cloudiness vs. tropospheric heat source Q1 (unit: W/m2, orange dots). The tropospheric heat source is integrated from 1000 hPa to 100 hPa over the box region using Eq. (2). (c) The ratio of the increment of cloudiness during 1948-2003 and the climatology mean

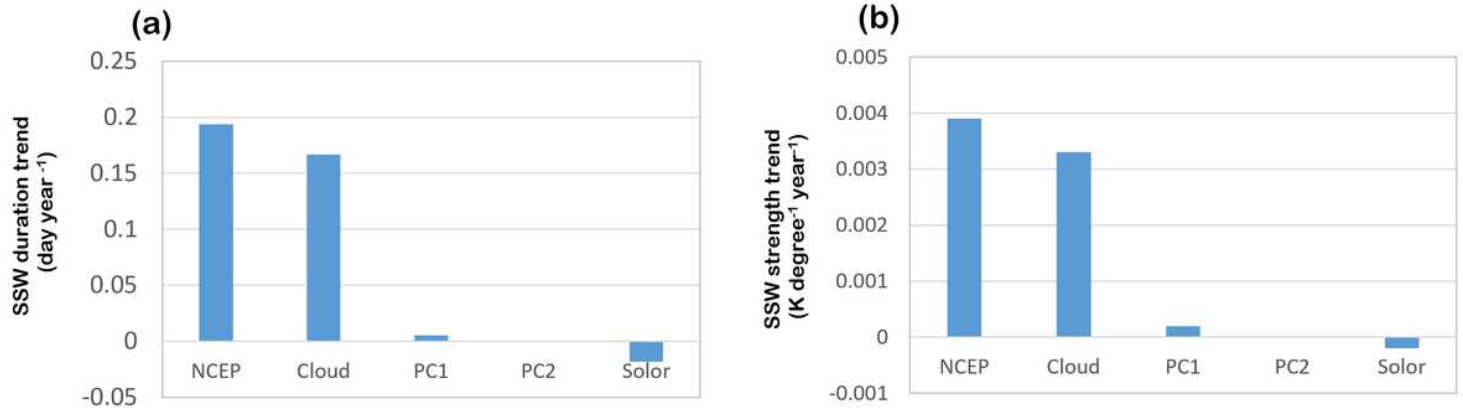

Figure 5

Contributions of different independent variables on the trends of (a) SSW duration (unit: day/yr) and (b) SSW strength (unit: K/ degree /yr). The trends are calculated in the period of 1948-2003. A multiple regression model adopted to calculate contribution is illustrated in the method section

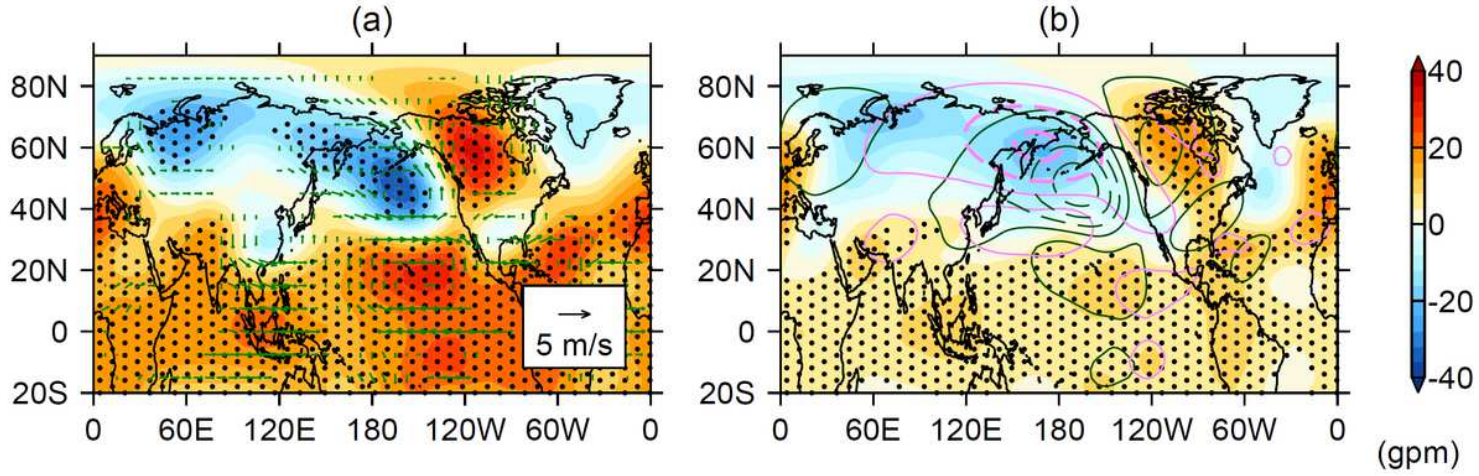

Figure 6

(a) Patterns of 200 hPa geopotential height (unit: gpm; color shadings) and winds (unit: m s−1; vectors) regressed on the standardized winter cloudiness in Fig. 3b. (b) Patterns of 200 hPa geopotential height regressed on the standardized SSW duration index in Fig. 1a. The contours in pink and green colors are representing the patterns of geopotential height anomalies regressed on WP and PNA teleconnections, in which the intervals are 20 gpm. The regions of dots exceed 99% confidence level. Note: The designations employed and the presentation of the material on this map do not imply the expression of any opinion whatsoever on the part of Research Square concerning the legal status of any country, territory, city or area or of its authorities, or concerning the delimitation of its frontiers or boundaries. This map has been provided by the authors.

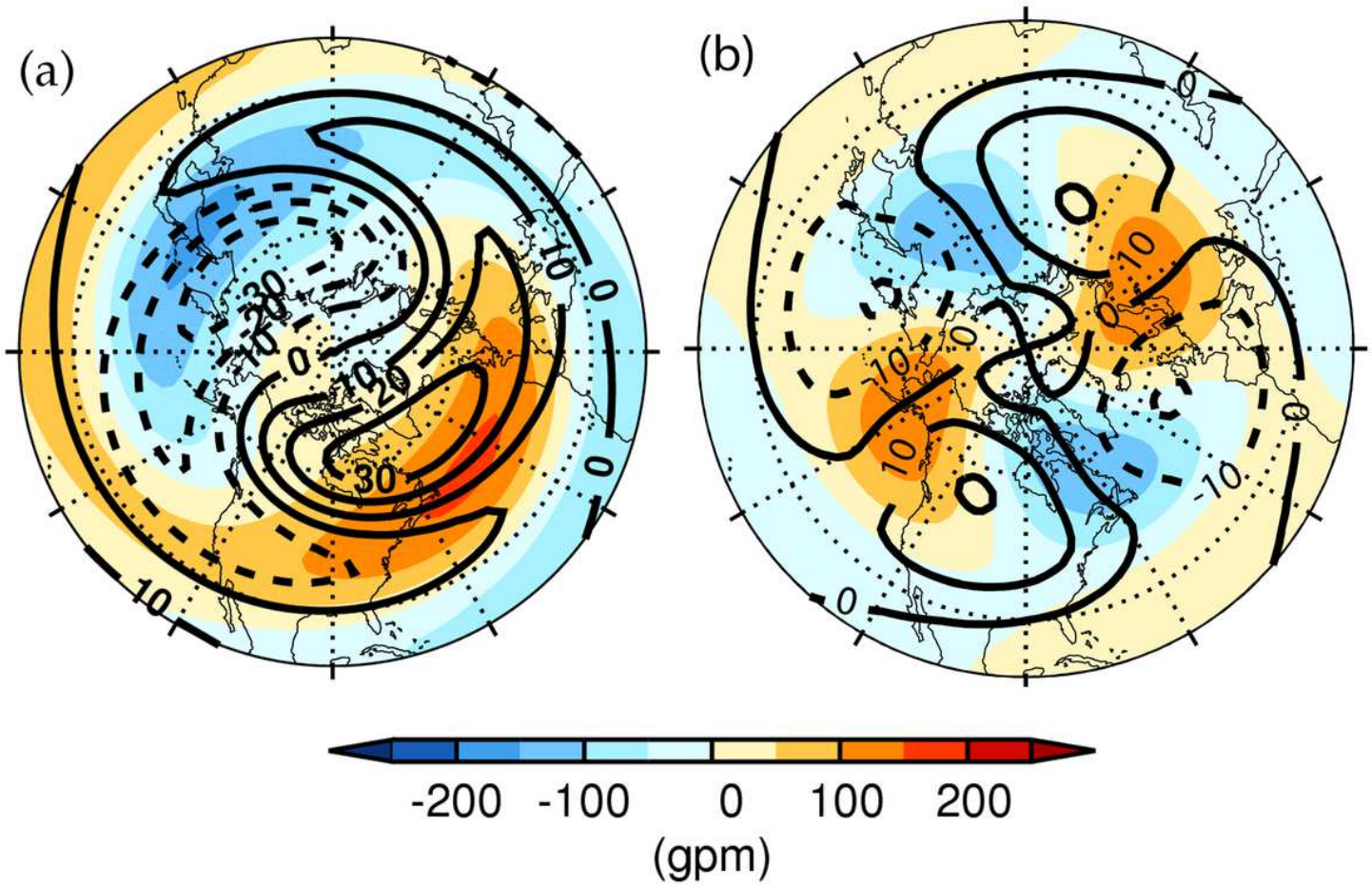

Figure 7

(a) planetary wave 1 (PW1) and (b) planetary wave 2 (PW2) components of the regressed geopotential height field in Fig. 6a. Black contour lines with the intervals of ± 10, ± 20, ± 30 gpm. The color-filled contours show the climatological pattern of PW1 and PW2. Note: The designations employed and the presentation of the material on this map do not imply the expression of any opinion whatsoever on the part of Research Square concerning the legal status of any country, territory, city or area or of its authorities, or concerning the delimitation of its frontiers or boundaries. This map has been provided by the authors.

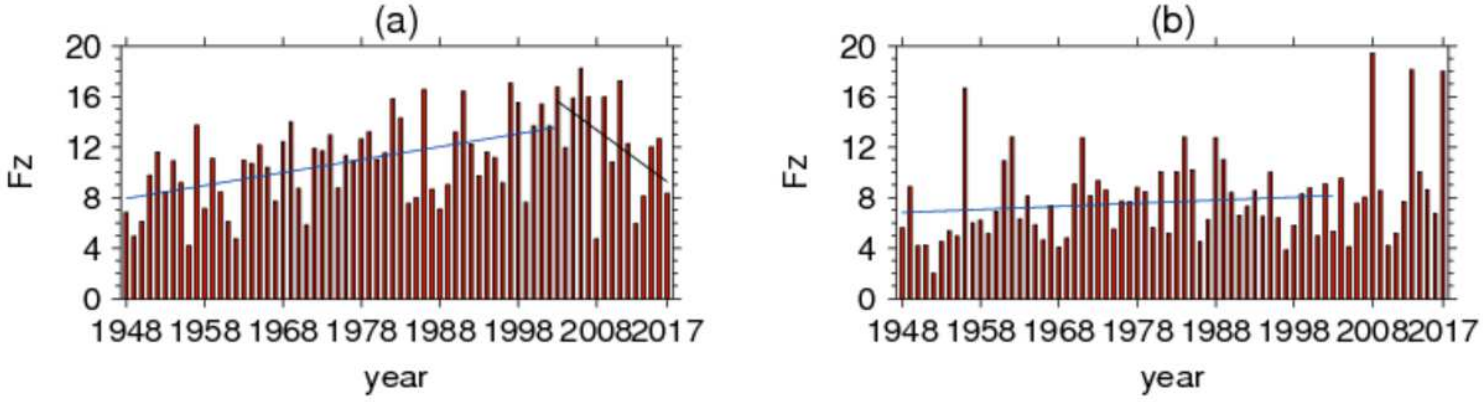

Figure 8

The time series of the winter F(z) (unit: 104m3s−2) at 100 hPa over the latitude band of 45°N–90°N associated with (a) PW1 and (b) PW2 components derived from the NCEP/NCAR reanalysis data. The blue line is the trend line from 1948 to 2003, and the black line is the trend line from 2004 to 2017

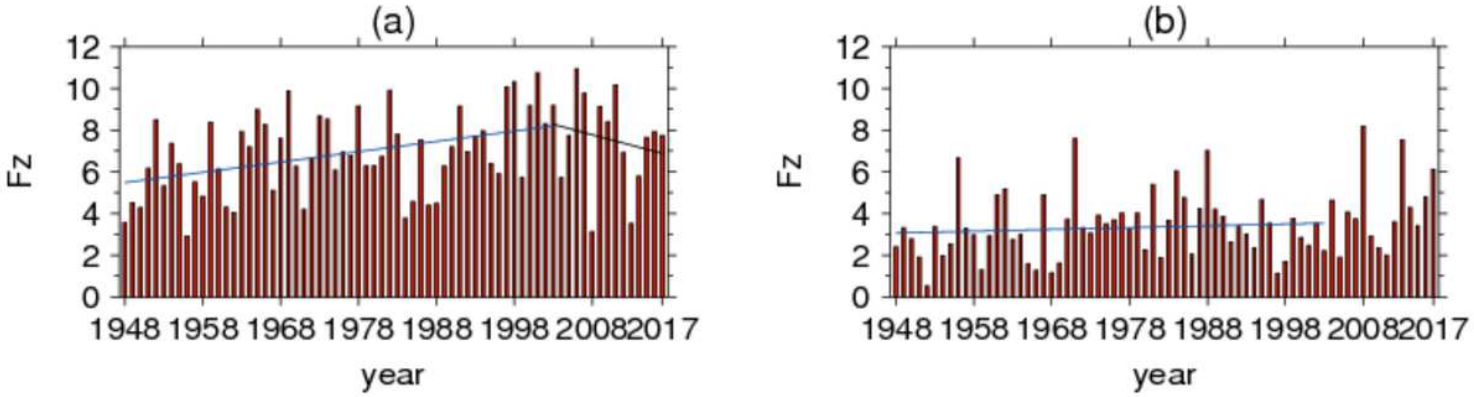

Figure 9

The time series of the winter F(z) (unit: 104m3s−2) at 20 hPa over the latitude band of 45°N–90°N associated with (a) PW1 and (b) PW2 components derived from the NCEP/NCAR reanalysis data. The blue line is the trend line from 1948 to 2003, and the black line is the trend line from 2004 to 2017

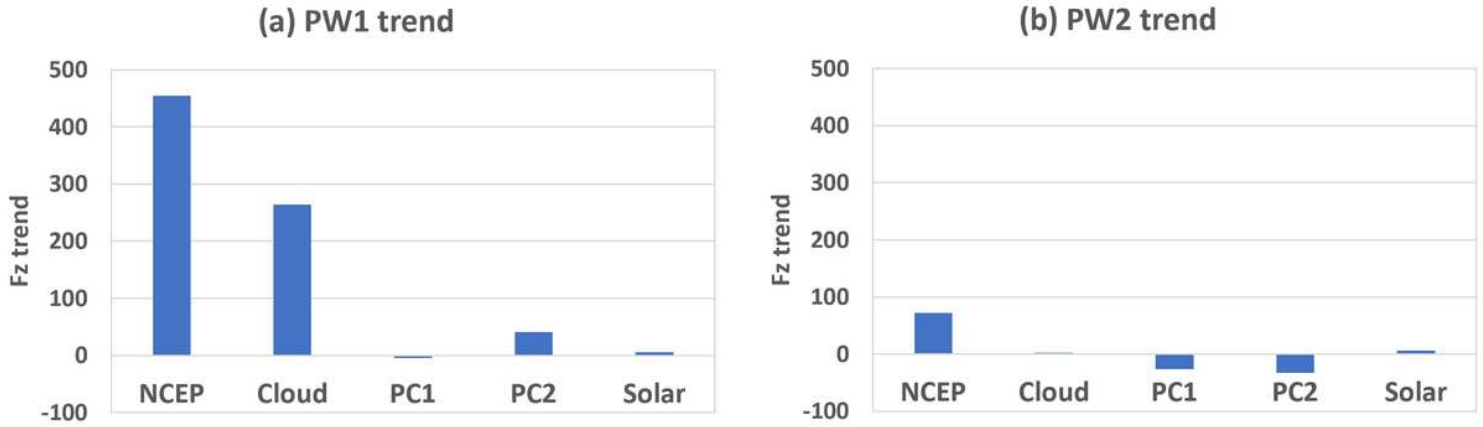

Figure 10

Contributions (unit: m3s−2/year) of different independent variables on the trends of (a) PW1 and (b) PW2 at 20 hPa. The trends are calculated in the period of 1948-2003. The independent variables are the same as in Fig. 5